Hindawi
International Journal of Photoenergy
Volume 2021, Article ID 6632180, 12 pages
https://doi.org/10.1155/2021/6632180

Research Article

The Role of Silicon Heterojunction and TCO Barriers on the Operation of Silicon Heterojunction Solar Cells: Comparison between Theory and Experiment

Yaser Abdulraheem,[1] **Moustafa Ghannam**,[1] **Hariharsudan Sivaramakrishnan Radhakrishnan**,[2] **and Ivan Gordon**[2]

[1]*EE Department, Kuwait University, P.O. Box 5969, Safat 13060, Kuwait*
[2]*Imec, Kapeldreef 75, 3001 Leuven, Belgium*

Correspondence should be addressed to Yaser Abdulraheem; yaser.abdulraheem@ku.edu.kw

Received 30 November 2020; Accepted 4 March 2021; Published 16 March 2021

Academic Editor: Jinn Kong Sheu

Photovoltaic devices based on amorphous silicon/crystalline silicon (a-Si:H/c-Si) heterojunction interfaces hold the highest efficiency as of date in the class of silicon-based devices with efficiencies exceeding 26% and are regarded as a promising technology for large-scale terrestrial PV applications. The detailed understanding behind the operation of this type of device is crucial to improving and optimizing its performance. SHJ solar cells have primarily two main interfaces that play a major role in their operation: the transparent conductive oxide (TCO)/a-Si:H interface and the a-Si:H/c-Si heterojunction interface. In the work presented here, a detailed analytical description is provided for the impact of both interfaces on the performance of such devices and especially on the device fill factor (FF). It has been found that the TCO work function can dramatically impact the FF by introducing a series resistance element in addition to limiting the forward biased current under illumination causing the well-known S-shape characteristic in the I-V curve of such devices. On the other hand, it is shown that the thermionic emission barrier at the heterojunction interface can play a major role in introducing an added series resistance factor due to the intrinsic a-Si:H buffer layer that is usually introduced to improve surface passivation. Theoretical explanation on the role of both interfaces on device operation based on 1D device simulation is experimentally verified. The I-V characteristics of fabricated devices were compared to the curves produced by simulation, and the observed degradation in the FF of fabricated devices was explained in light of analytical findings from simulation.

1. Introduction

Solar cell devices based on hydrogenated amorphous silicon/crystalline silicon (a-Si:H/c-Si) heterojunction (SHJ) experience relatively high open-circuit voltages (V_{OC}) and short-circuit currents (J_{SC}) leading to high conversion efficiencies (η) exceeding 26% when combined with Interdigitated Back Contact (IBC) technology [1]. Reduced optical losses at the front side attributed to the IBC architecture and the relatively low recombination losses attributed to the high passivation quality of the SHJ (a-Si:H/c-Si) interfaces have been accredited as the main reasons behind such a high efficiency. Such structures build upon the improved emitter efficiency of a-Si:H/c-Si bipolar transistors [2] and original solar cells with the so-called heterojunction with intrinsic thin layer (HIT®) developed by the Sanyo group in 1992 [3]. The main approach adopted by the Sanyo group to reduce interfacial recombination losses was to introduce a thin intrinsic a-Si:H (a-Si:H(i)) layer between 5 and 8 nm in thickness in between the c-Si substrate and the highly doped a-Si:H layer where this intrinsic buffer layer would lead to high-quality passivation [3–5].

However, a detailed analysis of the SHJ interface has revealed that excellent passivation mainly arises from a strong inversion layer within the c-Si substrate, invoked by Fermi potential differences due to energy band

discontinuities in the presence of chemical passivation that is achieved due to the high-quality interface between the c-Si substrate and the a-Si:H(i) layer [6, 7]. It has been elucidated by Ghannam et al. that if the inversion layer carrier density is severely impacted, then the SHJ device performance will deteriorate despite the fact that high chemical passivation is present due to the a-Si:H(i) buffer layer. The presence of this inversion layer inside the c-Si substrate close to the a-Si:H/c-Si interface has been experimentally verified and examined in the past [8–10].

It has also been shown in detail that factors influencing this inversion layer can have a detrimental effect on the performance of the device including strong degradation in the fill factor (FF) and a reduction in the open-circuit voltage (V_{OC}) [11]. In SHJ devices, the FF is of special concern since the utilization of an intrinsic amorphous silicon layer causes significant series resistance effects that have been attributed as the main cause for FF degradation [1].

It has recently been demonstrated that the FF is influenced by properties of the thermionic emission barrier that is established at the a-Si:H/c-Si interface due to energy band discontinuities. This barrier plays a major role in the performance of SHJ devices as demonstrated by means of theoretical device simulations which revealed that properties of the thermionic emission barrier such as the Richardson constant, barrier height, and temperature can impact the FF since this barrier becomes critically responsible for carrier transport across such interfaces [12, 13]. Other models have also suggested an additional transport mechanism related to quantum tunneling [14, 15].

On the other hand, an inadequate work function (WF) difference between the a-Si:H layer and the transparent conductive oxide (TCO) layer that acts as a front side (or rear side) contact can also have a detrimental effect on both the FF and V_{OC}. This effect becomes more pronounced when the a-Si:H layer is of relatively low doping and/or is ultrathin.

In principle, heavy doping in the a-Si:H layer should lead to proper device operation, where the impact of the thermionic emission barrier or TCO Schottky barrier due to an inadequate work function is minimized. But in practice, this is not effectively achieved where the a-Si:H layer might end up with lower effective doping due to free carrier capture by dangling bonds within a-Si:H layer [16, 17].

The purpose of the current work is to separately distinguish the impact of the a-Si:H/c-Si and TCO/a-Si:H interfacial properties on device performance. In the work presented, an a-Si:H (p+)/a-Si:H(i)/c-Si(n) structure was simulated using the AFORS-HET device simulator. The impact of an inadequate TCO work function (WF_{TCO}) and the effect of the thermionic emission barrier on device performance were revealed by simulating the I-V characteristics of two structures. The properties of the two structures simulated were chosen to emphasize the role of both the TCO and heterojunction interfaces on device operation and are representative of devices with high-level doping and moderate-to-low-level doping of the a-Si:H(p) layer.

The simulated I-V characteristics both in the dark and under illumination were used to separate the impact of the TCO/a-Si:H(p^+) interface (Schottky barrier interface) from the effects of the a-Si:H(i)/c-Si interface (thermionic emission barrier interface) on device behavior.

To further confirm the results of device simulation, several SHJ devices were fabricated with different dopant concentrations in the a-Si:H(p) layer and their I-V profiles in the dark and under illumination were measured to provide verification and validation for the device simulation results. A two-diode circuit model was also used to extract the effective series resistance values for the experimental devices under different operational conditions.

2. Device Simulation

Two device structures (SHJ1 and SHJ2) have been modeled using the AFORS-HET numerical simulation tool developed by Helmholtz-Zentrum Berlin [18]. The two structures are exactly identical except for the doping concentration in the a-Si:H(p^+) layer with values of $1 \times 10^{19}\,cm^{-3}$ and $1 \times 10^{20}\,cm^{-3}$ for SHJ1 and SHJ2, respectively. The SHJ device structure under study is shown Figure 1 and material parameters used in the simulations are outlined in Table 1. A 200 μm crystalline silicon (c-Si) substrate with n-type doping of $N_D = 1.5 \times 10^{16}\,cm^{-3}$ is used with an ideal ohmic back contact. The front of the c-Si substrate, which acts as the base for the photovoltaic device, is covered by a 5 nm a-Si:H(i) intrinsic buffer layer. The interface between the a-Si:H(i) buffer layer and the c-Si(n) base is modeled as a thermionic emission barrier. On top of the buffer layer, a 10 nm highly doped p-type a-Si:H(p^+) layer is placed acting as the emitter for the device. On top of the emitter layer, a TCO layer is placed acting as the front contact and the optical window at the same time. The TCO/a-Si:H(p^+) interface is modeled as a Schottky barrier and is mainly controlled by the work function difference between the two sides of the interface [19].

An inversion layer consisting of a high hole concentration is established in the c-Si substrate adjacent to the heterointerface as a result of energy band offsets that arise from electron affinity and band gap differences between amorphous silicon and crystalline silicon, where the peak hole concentration (reflecting a stronger inversion layer) becomes higher for a higher active doping in the a-Si:H(p^+) layer. From previous investigations [7], it has been established that any factor negatively impacting the inversion layer would have a detrimental impact on cell performance causing mainly the cell's open-circuit voltage V_{OC} to drop. In addition, the electric field that is established around the a-Si:H/c-Si interface extends into the a-Si:H(i) buffer layer and can reach into the a-Si:H(p^+) layer depending on the amount of active doping inside that layer [13]. At thermal equilibrium, the electric field established causes a majority carrier spillover into the intrinsic buffer layer by balancing the diffusion of holes towards the emitter. The hole spillover into the intrinsic layer influences its conductivity, which in turn has a direct impact on the contribution of the intrinsic buffer layer on the effective series resistance of the device.

In addition to the existence of a strong inversion layer, two other factors can also influence the operation of SHJ solar cell devices, impacting the FF and series resistance (R_{Series}). These factors include the thermionic emission

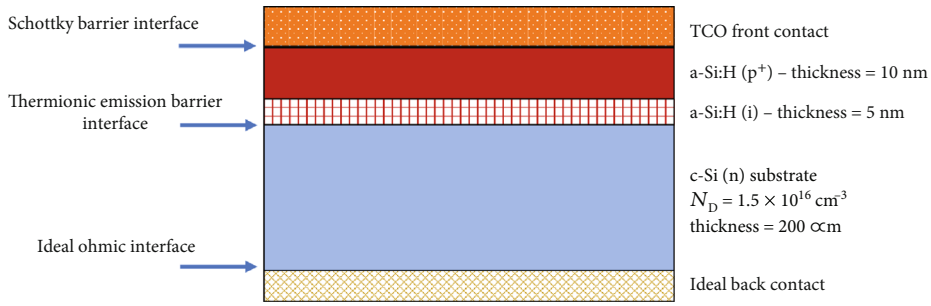

Figure 1: Structure of the modeled SHJ device.

Table 1: Parameter values used in the simulation of the SHJ devices under study.

Parameter	Value
a-Si:H band gap, $E_{g,a-Si}$	1.72 eV
c-Si band gap, $E_{g,c-Si}$	1.124 eV
a-Si:H electron affinity, χ_{a-Si}	3.9 eV
c-Si electron affinity, χ_{c-Si}	4.05 eV
Doping concentration for a-Si:H(p$^+$) sample SHJ1—$N_{aSi^{-1}}$	1×10^{19} cm^{-3}
Doping concentration for a-Si:H(p$^+$) sample SHJ2—$N_{aSi^{-2}}$	1×10^{20} cm^{-3}
Minimum bulk dangling bond defect density	1.385×10^{16} cm^{-3} eV^{-1}
Peak dangling bond defect density at the a-Si:H(i)/c-Si interface	1×10^{10} cm^{-2} eV^{-1}
Richardson constant ($A*$) for the thermionic emission barrier	9.56 A K^{-2} cm^{-2}
Conduction band offset between a-Si and c-Si (ΔE_c)	0.15 eV
Valence band offset between a-Si and c-Si (ΔE_v)	0.446 eV

barrier at the a-Si:H(i)/c-Si heterointerface and the Schottky barrier established at the a-Si:H(p$^+$)/TCO interface [13, 15] .

The simulation study here is conducted over two parts. In the first part of the study, FF degradation due to effects of the Schottky interface between the TCO and the a-Si:H(p$^+$) layer is considered. In the second part, the impact on the FF due to the thermionic emission barrier is considered. For that part, the TCO/a-Si:H(p$^+$) interface is taken as an ideal "flatband" ohmic contact.

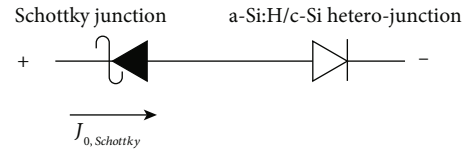

Figure 2: Simple diode model for the forward biased SHJ under dark (with $j_{ph} = 0$) or under low-level injection conditions (with a positive j_{ph}).

2.1. Impact of the TCO/a-Si(H) Interface. In this part of the study, the TCO work function is altered and the impact of such a variation on the FF is studied for two doping concentrations in the a-Si:H(p$^+$) layer. This condition is set in order to decouple the effects of the two barriers and get to a better understanding of their impact individually on the FF. It should also be noted, following earlier work [7], that bulk defects in amorphous silicon have been included into the simulation following two Gaussian profiles, acceptor-type and donor-type, with for each type, a peak concentration is equal to the doping concentration in the layer. As for a-Si:H/c-Si interface defects, also two Gaussian profiles are assumed with a peak concentration of 1×10^{10} cm^{-2} eV^{-1}, which reflects technologically achievable high-quality chemical passivation at the interface [20]. Additionally, both Shockley-Read-Hall and Auger recombination mechanisms are considered, while band gap narrowing effects were neglected for the bulk c-Si layer. The simulation was conducted under both dark and AM1.5G illumination conditions. In addition, reflection losses at the front side and losses due to parasitic absorption in the TCO layer were ignored.

Dark I-V characteristics were simulated by applying biasing to the devices with the back contact used as the bias reference. Under such a bias condition, the a-Si:H(p+)/a-Si:H(i)/c-Si(n)pn junction becomes forward biased, while the TCO/a-Si:H(p$^+$) junction becomes reverse biased (see Figure 2).

If an ideal TCO is considered (flatband conditions are invoked such that $WF_{TCO} = WF_{a-Si}$), then the TCO/a-Si:H is at flatband condition such that the Schottky junction is ignored. As has been mentioned above, to isolate the impact of the TCO work function on the shape of the I-V curve, the thermionic emission transport mechanism across the a-Si:H/c-Si heterointerface is not considered in the first part of the simulation under dark conditions and the current

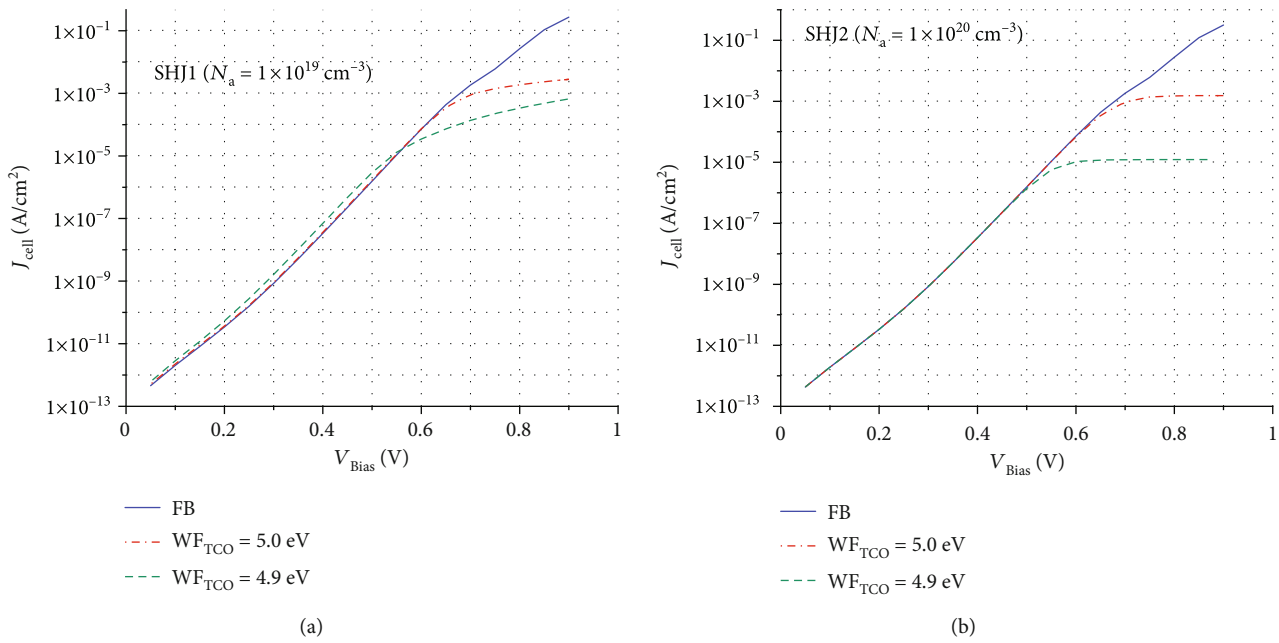

FIGURE 3: Simulated I-V characteristics for SHJ1 (a) and SHJ2 (b) under dark conditions with WF_{TCO} = 5.1 eV (close to flatband condition), 5.025 eV and 4.96 eV. A drift-diffusion model is invoked, and thermionic emission across the heterointerface is disabled.

characteristics are simulated using the drift-diffusion carrier transport model. Three different TCO work function (WF_{TCO}) values are considered in simulating the I-V curves, one with a flatband condition, one with a WF_{TCO} = 5.025 eV, and one with WF_{TCO} = 4.96 eV. Note that the value of the work function for the flatband condition is adjusted to match the doping level in the a-Si:H(p^+) layer.

As can be seen in Figure 3, the I-V curves for both devices under simulation exhibit a normal behavior for a forward biased PN junction for the flatband case. However, once a significant work function difference is invoked, the reverse biased Schottky junction sets the upper limit for the current flowing through the device. If the current flowing has a value smaller than the Schottky junction reverse saturation current, $j_{0Schottky}$, then the normal I-V exponential behavior prevails, but once the overall current approaches $j_{0Schottky}$, then the I-V characteristics will experience saturation at that value since the reverse biased Schottky junction behavior will dominate. This current saturation behavior is clearly seen in Figure 3 when the values of WF_{TCO} = 5.025 eV and WF_{TCO} = 4.96 eV are used. It is also noticed that the saturation behavior strictly occurs at $j_{0Schottky}$ for the higher doping device SHJ2 as is shown in Figure 3(b) as compared to a leaky saturation for the lower doping device, SHJ1 (Figure 3(a)). In a cell with relatively lower doping in the a-Si:H(p^+) layer, several conditions play a role in shaping the I-V curve at moderate-to-high biases when WF_{TCO} is relatively small. For instance, high-level injection occurs early in such devices where the majority carrier type changes from holes to electrons, and as a result, the TCO Schottky barrier is eliminated which prevents the current from saturating at $j_{0Schottky}$ as is shown in Figure 3.

Figures 4(a) and 4(b) show the I-V behavior under AM1.5G illumination for the SHJ1 and SHJ2 devices, respectively. Under illumination, a photogenerated current moves towards the TCO/a-Si:H Schottky contact and flows in the forward direction relative to the Schottky diode. At smaller WF_{TCO} values, the voltage drop on the Schottky diode due to the flow of such a current enhances the forward bias on the pn junction which increases its forward current and shifts the maximum power point to smaller values leading to a degradation of the cell FF, as can be seen in Figure 4.

Equivalently, when the cell is subjected to illumination, splitting in the quasi-Fermi levels at short-circuit condition is observed causing a potential difference for the carriers on both sides of the heterojunction. The nature and source of this potential difference (referred to as the short-circuit voltage V_{SC}) has been previously explained in an earlier report [21]. The presence of V_{SC} can be linked to an additional series resistance that will exist as the photogenerated current crosses the heterointerface towards the emitter which additionally impacts the FF negatively. This effect is more pronounced for relatively low values of WF_{TCO} and lower a-Si:H(p^+) doping levels. The value of the additional series resistance due to the short-circuit voltage drop can be calculated by extracting the short-circuit voltage V_{SC} from the split in the quasi-Fermi levels obtained from the simulated energy band diagram for both cells. An example of the energy band diagram for SHJ1 under illumination and at short-circuit conditions is shown in Figure 5. It should be noted that the value of V_{SC} is calculated assuming a drift-diffusion model across the a-Si:H/c-Si heterointerface. The value of the short-circuit series resistance R_S is found by dividing the extracted V_{SC} by the short-circuit current and reveals a value for R_S in the range of 2 Ω cm^2 for both heavily and moderately doped cells. The value of R_S in this case depends on the TCO work function as has been mentioned above, while the value of the short-circuit voltage, V_{SC}, depends on the position of the quasi-Fermi levels which in

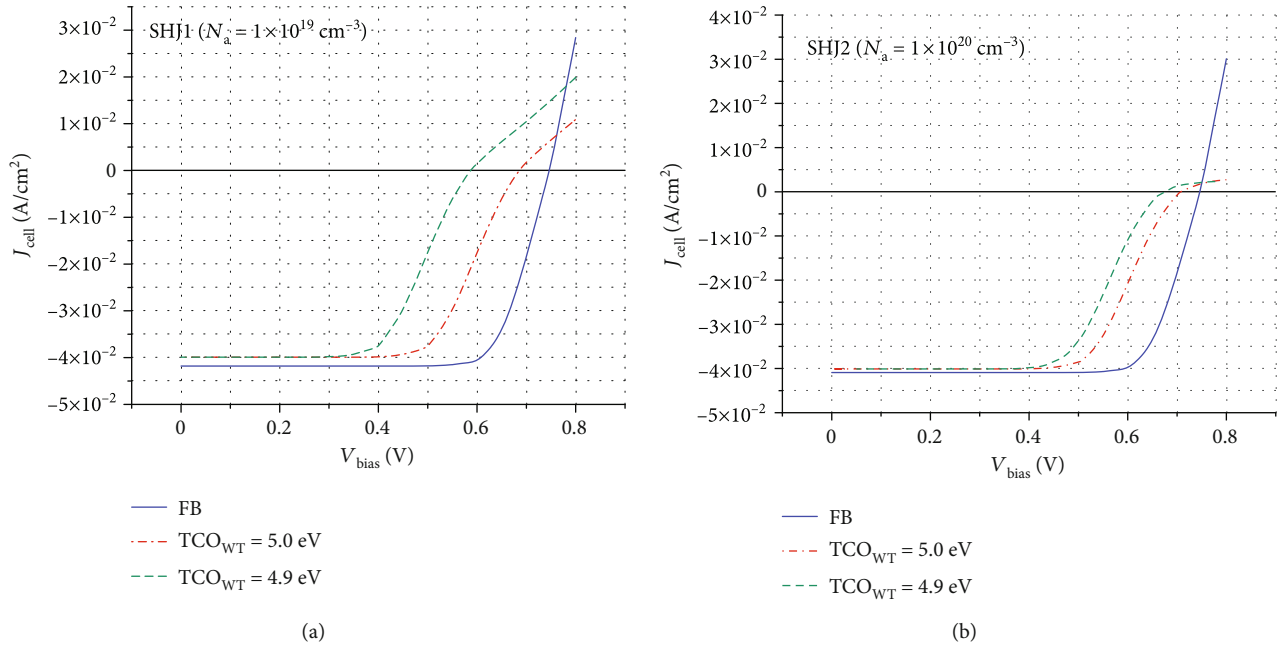

FIGURE 4: Simulated I-V characteristics under illumination for the two devices under study (a) SHJ1 and (b) SHJ2 with a drift-diffusion model (thermionic emission across the heterointerface is disabled).

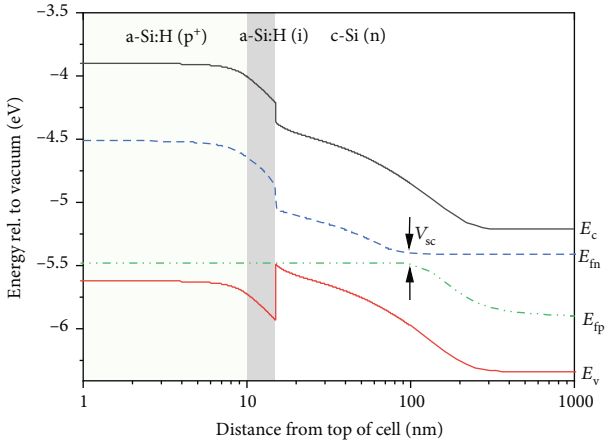

FIGURE 5: Energy band diagram for SHJ1 structure under illumination. Note that thermionic emission across the SHJ is ignored.

turn are highly impacted by the Schottky diode potential difference present at the TCO side of the device.

Table 2 summarizes extracted values of V_{OC}, FF, J_{SC}, and efficiency for the two simulated samples, SHJ1 and SHJ2, along with values of R_S that are calculated for the different values of WF$_{TCO}$.

At relatively high values of WF$_{TCO}$, band bending due to the Schottky barrier at the TCO/a-Si:H interface does not extend deep into the a-Si:H layer. On the other hand, at low values of WF$_{TCO}$, the space charge electric field created by band bending at the TCO/a-Si:H interface due to the Schottky barrier penetrates deeper into the a-Si:H(p$^+$) layer, especially when the doping level is low. That electric field may merge with the electric field present at the a-Si:H/c-Si heterointerface which can consequently cause a lowering of the barrier at the heterointerface. This negatively impacts the inversion layer peak hole concentration and leads to a lower V_{OC} and a larger emitter dark current which has a detrimental impact on the FF. This phenomenon becomes less significant for thicker a-Si:H(p$^+$) layers and for layers with relatively higher doping concentrations since a higher majority carrier concentration in the a-Si:H(p$^+$) layer can block the penetration of the electric field created at the Schottky interface and consequently the latter will have a lesser impact on the inversion layer.

Beyond V_{OC}, the current changes direction and the Schottky diode becomes reverse biased which saturates the current at the value of $j_{0Schottky}$, similar to the behavior of the cells under dark conditions which clearly explains the S-shape in the I-V characteristics that has been observed previously in SHJ devices with relatively low doping [22]. An explanation of such a behavior due to a rectification effect at the TCO/a-Si:H interface has also been reported in the past

TABLE 2: Values of V_{OC}, FF, J_{SC}, and cell efficiency extracted from the I-V curves of the two simulated structures SHJ1 and SH2 for different values of WF$_{TCO}$.

Sample	WF$_{TCO}$ (eV)	V_{OC} (mV)	FF (%)	J_{SC} (mA/cm^2)	η (%)	R_S (Ω cm^2)
SHJ1	FB	747	78	41.8	24.4	1.97
	5.025	685	68.8	39.9	18.8	5.05
	4.90	586	64.5	39.9	15.1	7.50
SHJ2	FB	746	78.2	40.9	23.9	1.94
	5.025	706	69.1	40.1	19.5	5.00
	4.90	611	63.9	40.1	15.7	7.10

[23]. The S-shape behavior in the I-V curve for the devices under study is clearly depicted in Figure 4.

2.2. Impact of the a-Si(H)/c-Si Interface. The second part of the simulation is focused on the impact of the thermionic emission barrier at the a-Si:H/c-Si interface on the I-V characteristics of SHJ devices. Unless otherwise stated, device structure and simulation parameters are maintained as in the first part of the theoretical study. For these simulations, a flatband condition at the TCO/a-Si:H interface is invoked removing the Schottky barrier effect on the I-V characteristics. The size of the thermionic emission barrier depends on the energy band discontinuities and positions of the Fermi levels on both sides of the heterointerface, which in turn are highly controlled by doping levels. It has been reported earlier that the inclusion of a thermionic emission model as the main transport mechanism across the heterointerface will lead to an enhanced V_{SC} which is a result of hole pile-up and reflection at the barrier [13, 24].

Under thermal equilibrium, spillover of free carriers from the heavily doped a-Si:H(p) layer into the a-Si:H(i) layer under the presence of an equilibrium electric field created at the heterointerface would establish a relatively high free hole concentration within the a-Si:H(i) layer maintaining a low series resistance in the dark. On the other hand, under illumination, some photogenerated holes cannot cross the thermionic emission barrier and hence reflect and pile up at the heterointerface [13]. The pile-up of holes close to the heterointerface due to the thermionic emission barrier will cause an additional electric field that would deplete the a-Si:H(i) buffer layer and hence increase the layer resistance. This substantial increase in the effective series resistance would lead to further degradation in the I-V characteristics and have a direct impact on the FF. This effective series resistance has a smaller value for the more heavily doped sample, SHJ2, due to a larger majority carrier spillover into the intrinsic buffer layer, leading to this layer having a partially higher conductivity. Indeed, this behavior is clearly shown in the simulated I-V characteristics of SHJ1 and SHJ2 under illumination, as shown in Figure 6, where the more heavily doped sample SHJ2 does not exhibit a large degradation in its FF as opposed to the case for SHJ1. Table 3 summarizes the illuminated I-V characteristics for SHJ1 and SHJ2 when the thermionic emission model is invoked.

Under illumination, peak hole concentration and hole pile-up at the heterointerface decreases under forward bias conditions. This leads to a decrease in the series resistance of the intrinsic buffer layer [13]. It is very clear that the bias-dependent enhancement and bias dependence of the series resistance have no major effect on the open-circuit voltage which remains more or less constant at a value around 748 mV for both heavily doped and moderately doped cells, as shown in Figure 6.

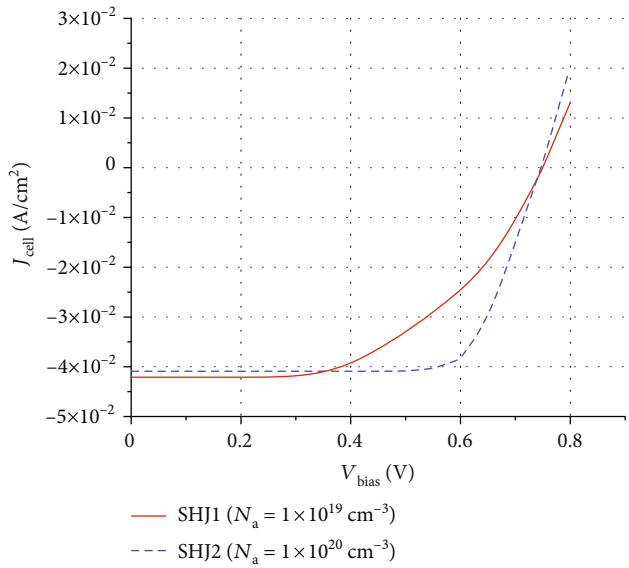

Figure 6: I-V characteristics under illumination for SHJ1 and SHJ2 under thermionic emission transport conditions and with a flatband TCO interface.

Table 3: Device I-V parameters extracted for cells SHJ1 and SHJ2 under illumination with the thermionic emission model.

Sample	V_{OC} (mV)	J_{SC} (mA/cm^2)	FF (%)	η (%)
SHJ1	748	42.1	52.3	16.5
SHJ2	748	40.9	75.3	23

3. Experimental Verification

3.1. Details of Device Fabrication and Characterization. N-type, 180 μm thick, 4.2 Ω cm, (100) Czochralski (Cz) wafers were used for the fabrication of SHJ solar cells. The solar cell cross section and the process flow, depicted in Figure 7, are similar to that reported in our previous work [25].

While the simulated cell structure differs from that of the fabricated cell structure, the impact of the emitter contact interfaces (TCO/p-a-Si:H/i-a-Si:H/c-Si) on the device characteristics would be similar in both cases, and as such, the experimental observations can be used to qualitatively validate the theoretical findings from the device simulations of Section 2. The as-cut wafers were etched to remove saw damage and were subsequently textured in potassium hydroxide (KOH) at 80°C to produce a random pyramid texture on both surfaces of the wafers. The wafers were then laser-cut to squares of size of 125 × 125 mm^2. These downsized wafers were then cleaned in ozonated water, followed by a diluted hydrofluoric acid (HF) solution.

Then, a stack of hydrogenated intrinsic and n-doped amorphous silicon (i/n$^+$ a-Si:H) layers with thicknesses of 5 nm and 7 nm, respectively, was deposited on the front side, using plasma-enhanced chemical vapor deposition (PECVD). On the rear side, a stack of intrinsic and p-doped a-Si (i/p$^+$ a-Si:H) layers with thicknesses of 9 nm and 16 nm, respectively, was deposited. Silane (SiH_4) and hydrogen (H_2) were used as precursor gases for the a-Si:H deposition. The p-doping in the a-Si:H is achieved by additionally flowing 2% of trimethylborane (TMB) diluted in hydrogen (H_2) during the a-Si deposition process.

The doping level in the a-Si:H(p) was varied by changing the gas flow rate of 2% TMB (Q_{TMB}) with respect to that of

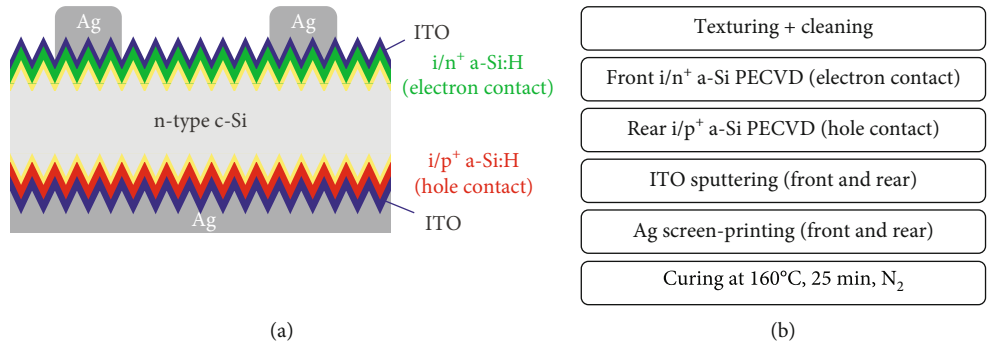

Figure 7: The cross-sectional schematic (a) and the process flow (b) of silicon heterojunction solar cells.

SiH_4 (Q_{SiH_4}). The different conditions used in this work are summarized in Table 4. For the reference condition, TMB 50/50, the $Q_{TMB} : Q_{SiH_4}$ ratio was 1 : 1, corresponding to 2% of TMB in SiH_4 in the gas mixture. This corresponds to a high doping level in the a-Si:H(p). To evaluate the effect of lower doping levels in the a-Si:H(p) layer on the transport characteristics of this heterocontact, three additional splits in the a-Si:H(p) layer depositions, with $Q_{TMB} : Q_{SiH_4}$ ratios of 1 : 5, 1 : 7.5, and 1 : 10, corresponding to 0.4%, 0.27%, and 0.2% of TMB in SiH_4 in the gas mixture, were also tested in this study. The H_2 flow rate (Q_{H_2}) was kept constant for all splits.

Minority carrier lifetime measurements were performed using the quasi-steady-state photoconductance (QSSPC) method to evaluate the passivation quality, while photoluminescence (PL) imaging was performed to evaluate the passivation uniformity. In the next step, the wafers were again cleaned in HF solution to remove any native oxide on the a-Si:H surfaces. Then, indium tin oxide (ITO) was deposited on both surfaces by DC sputtering through a shadow mask with an opening of $40 \times 40\,mm^2$, which defines the area of the cell. In this way, 4 cell areas are defined per wafer. Finally, screen printing of the front and rear contacts was done using a low-temperature Ag paste, which is cured at 160°C for ~25 min in N_2 in a belt furnace. The wafers were then again laser-diced to produce 4 individual cells from each wafer. A total of 8 cells were fabricated for each split. Illuminated current-voltage (I-V) measurements were then done using the AM1.5G spectrum in a solar simulator at 25°C, under 1 sun intensity, using an aperture area of $15.95\,cm^2$.

3.2. Device Performance Results. Minority carrier lifetime measurements show that wafers from all the splits exhibit excellent and similar surface passivation, as plotted in Figure 8, with lifetimes in the range of ~5-6 ms at an injection level of $10^{15}\,cm^{-3}$. After ITO deposition, the lifetimes drop to around 2.1-2.6 ms due to damage from sputtering. However, this passivation loss is fully recovered for most of the wafers during the curing step after screen printing, whereby the wafers are subjected to an 160°C anneal in N_2 for around 25 min. Thus, there are no major differences in terms of passivation quality between the different i/p^+ a-Si:H splits, indicating that the lower doping levels of the a-Si:H(p) layers used in this work do not affect the passivation quality adversely.

Table 4

(a) Gas flow rates of silane (Q_{SiH_4}) and 2% TMB in H_2 (Q_{H_2}) used for the deposition of p-a-Si:H, and the corresponding flow ratios and TMB % in SiH_4 in the gas mixture. The H_2 flow rate (Q_{H_2}) was kept constant

Split name		Gas flow rates (sccm) 2% TMB in H_2 (Q_{TMB})	Silane (Q_{SiH_4})	Q_{TMB}/Q_{SiH_4}	TMB % in SiH_4
TMB 50/50	Reference 1	50	50	1	2
TMB 10/50	Low doping 1	10	50	0.2	0.4
TMB 10/75	Low doping 2	10	75	0.13	0.27
TMB 10/100	Low doping 3	10	100	0.1	0.2

(b) Summary of the lowest, average, and best light I-V parameters of cells from the different splits of a-Si:H(p) devices

Split		Short-circuit current density, J_{SC} (mA/cm^2)	Open-circuit voltage, V_{OC} (mV)	Fill factor, FF (%)	Efficiency, η (%)
TMB 50/50	Lowest	35.1	729.5	76.8	19.7
	Avg	35.2	733	78.1	20.1
	Best	35.4	735	79.1	20.6
TMB 10/50	Lowest	34.9	738	65.7	16.9
	Avg	35.2	741	66.8	17.5
	Best	35.5	742	67.9	17.9
TMB 10/75	Lowest	35.0	705.8	66.7	16.5
	Avg	35.0	714	66.2	16.5
	Best	35.2	712	67.0	16.8
TMB 10/100	Lowest	35.3	702.3	66.1	16.4
	Avg	35.3	715	65.7	16.5
	Best	35.3	720	65.7	16.7

The FF and efficiency for all fabricated samples are plotted in Figures 9(a) and 9(b), respectively, while the lowest, best, and average light I-V cell parameters of the different

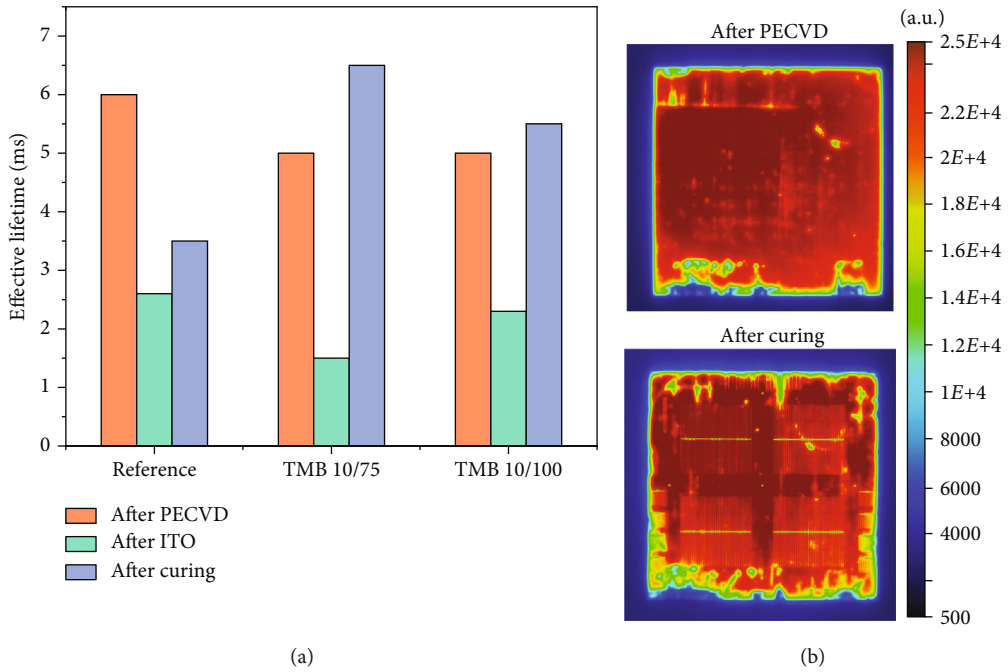

Figure 8: (a) Effective lifetime at the injection level of 10^{15} cm^{-3} for 3 different splits (as described in Table 4), after different processing steps, namely, PECVD, ITO sputtering, and curing after Ag screen printing. (b) Uncalibrated PL images of a wafer (reference split) after PECVD and after curing, exhibiting similar levels of passivation.

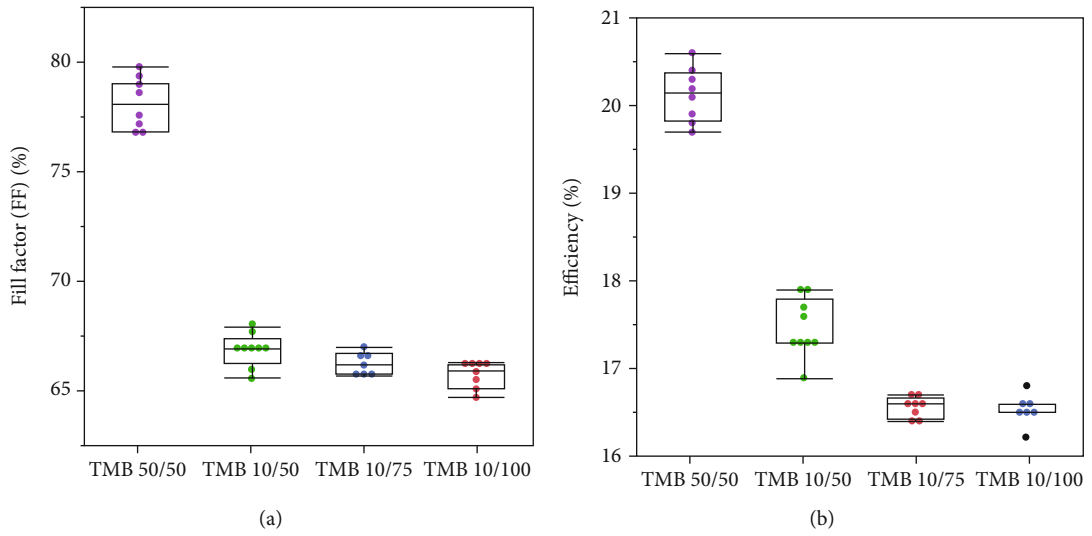

Figure 9: Box plots of the distribution of the fill factor (FF) and efficiency of the cells from the different splits.

splits are summarized in Table 5. Given that the i/p^+ a-Si:H emitter contact is implemented at the rear of the cell, there is no significant difference between the splits in terms of short-circuit current density (J_{SC}). On the other hand, as expected, the fill factor (FF) values of all the low doping splits, namely, TMB 10/50, TMB 10/75, and TMB 10/100, are considerably lower compared to those of the reference split (TMB 50/50). Similarly, the open-circuit voltage (V_{OC}) of the two lowest doping splits, TMB 10/75 and TMB 10/100, is significantly lower compared to the reference split, whereas the V_{OC} of the TMB 10/50 remains high, reaching >740 mV.

Table 5: Parameters used in fitting I-V curves with the two-diode model. The values of R_{Shunt} and R_{Series} are obtained from the fitting.

Sample	J_{01} (A/cm^2)	J_{02} (A/cm^2)	n_1	n_2	R_{Shunt} (MΩ cm^2)	R_{Series} (Ω cm^2)
TMB 10/50	2.75×10^{-14}	4.6×10^{-8}	1	2.79	0.8	1.8
TMB 50/50	1.75×10^{-14}	4.6×10^{-8}	1	2.79	0.8	1.8

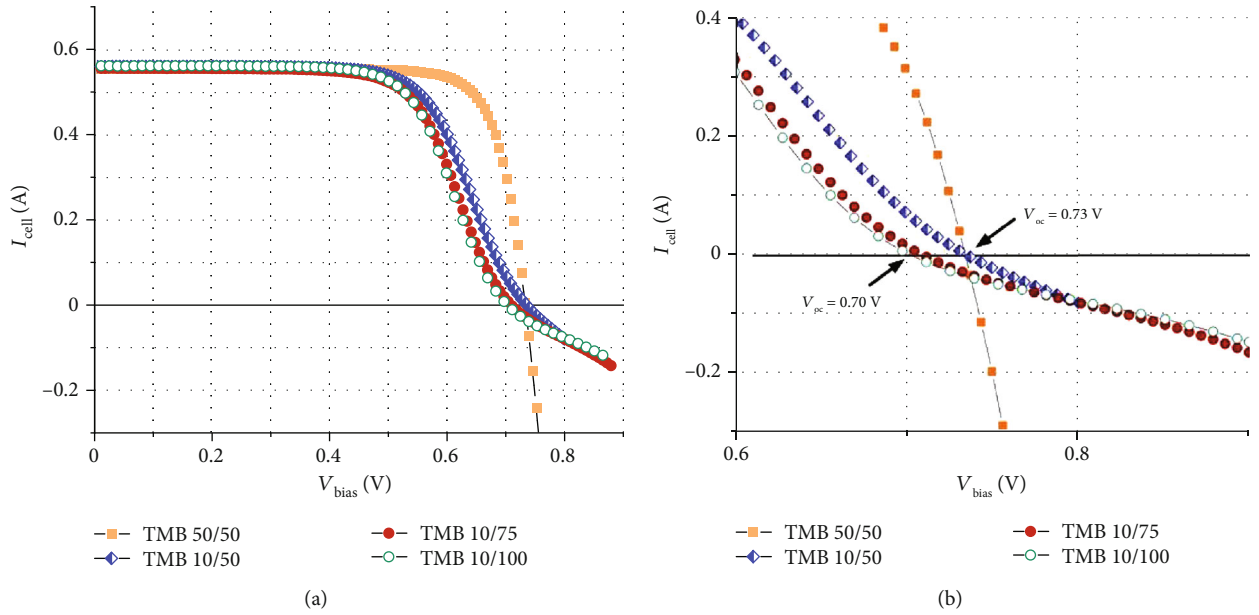

FIGURE 10: Light I-V characteristics of typical cells from the four different sample splits as described in Table 4. Panel (b) shows an expanded view close to the V_{OC} point of the same curves in (a). The arrows indicate the shift in the value of V_{OC}.

This can be clearly seen from the I-V characteristics of representative cells from the different splits under AM1.5 illumination plotted in Figure 10. Moreover, all low doping splits, TMB 10/50, TMB 10/75, and TMB 10/100, exhibit a strong S-shape close to the V_{OC} point.

All of these characteristics are explained qualitatively in light of the simulation results of Section 2. The S-shape in the light I-V characteristics for the low doping splits in Figure 10 is similar to that shown by simulations in Figure 4 and is indicative of a Schottky barrier at the TCO/a-Si:H(p^+) interface.

For the TMB 10/50 split, the degradation in device performance is only due to a lowering of the FF, while the V_{OC} remains high. This behavior is similar to that simulated in Figure 6, and implies that for this split, the transport characteristics are limited by the thermionic emission barrier at the a-Si:H/c-Si interface, and not the TCO/a-Si:H interface. However, when the doping level is dropped even further in the TMB 10/75 and TMB 10/100 splits, the V_{OC} is also adversely impacted in addition to the FF. This behavior is similar to that simulated in Figure 4, indicating that both the thermionic emission barrier at the a-Si:H/c-Si interface and the Schottky barrier at the TCO/a-Si:H interface affect the device characteristics.

Theoretical interpretations based on device simulation as described in Section 2 are used to further explain the FF degradation for two fabricated devices having two different doping levels in the a-Si:H(p^+) layer, namely, sample TMB 10/50 representing the sample with low doping and sample TMB 50/50 representing the sample with high doping. A two-diode model fit was used to extract an estimate of the cell series resistance. For both samples, I-V measurements in the dark and under AM1.5G illumination were carried out at 25°C. Both measurements along with a two-diode model fit are shown in Figures 11(a) and 11(b) for measurements in the dark and under illumination, respectively.

Fitting of the dark currents of both cells and parameter extraction were carried out using a MATLAB optimization code developed in-house. The MATLAB code is based on a two-diode model (Figure 12) and the with parameters displayed in Table 5. The R_{Series} and R_{Shunt} values are obtained through fitting with the experimental I-V curves shown in Figure 11.

Beyond 0.65 V, the dark current of TMB 10/50 shows an onset of saturation which is indicative of the presence of a Schottky contact, as is explained in Section 2. The current saturation does not appear in TMB 50/50 (heavily doped sample) which indicates that the TCO/a-Si:H contact suffers from current leakage inhibiting its saturation. One possible cause for such a saturation behavior can be due to a tunneling mechanism at the interface at high doping concentrations [15].

In the midvoltage range 0.2 V to 0.63 V, the dark current of both cells is almost perfectly matching the behavior of the two-diode model (excluding a Schottky contact) with the fitting parameters displayed in Table 5 and with the series resistance for both cells being at a value of 1.8 Ω cm^2.

The dark current in both cells is dominated by injection in the high-resistivity substrate, which explains the practically equal dark currents measured for both cells in the voltage range 0.2 V to 0.63 V with a very slight difference observed. This observation may be due to differences in carrier lifetimes or due to the difference in the doping levels in a-Si:H(p^+) layer. The deviation in the behavior of TMB 10/50 from the fit for biases higher than 0.65 V is due to the presence of the Schottky contact at the TCO/a-Si:H interface, which is not considered in the fit. The existence of such a Schottky contact justifies the presence of the S-shape in the

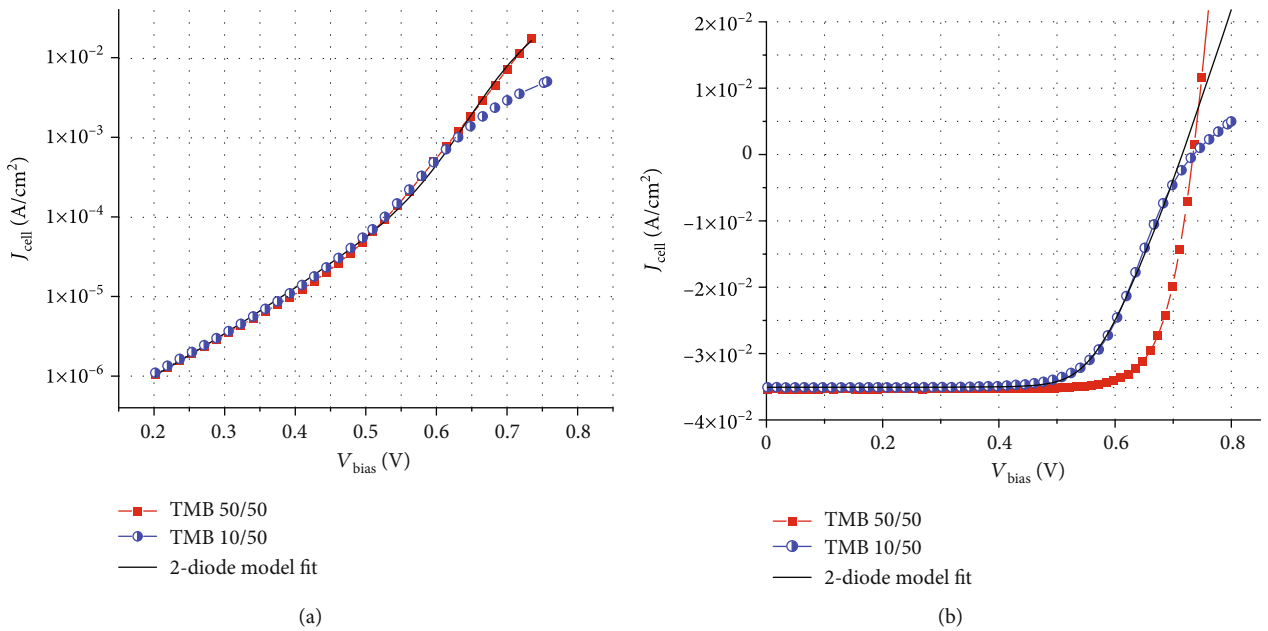

Figure 11: I-V characteristics for samples TMB 10/50 and TMB 50/50 under (a) dark conditions and (b) light conditions, both with the 2-diode model fitting.

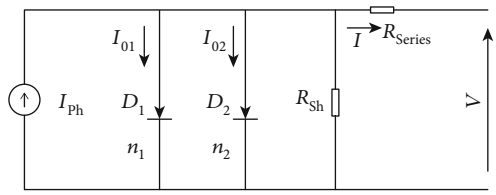

Figure 12: Schematic of the two-diode model used for the I-V curve fitting.

I-V characteristics under illumination for sample TMB 10/50 as shown in Figure 11(b).

On the other hand, the sample with high doping (TMB 50/50) does not show this effect, which agrees very well with the behavior of the dark current and the assumption of tunneling discussed above. Although current saturation in the I-V characteristics under illumination beyond V_{OC} confirms the presence of a Schottky diode in TMB 10/50, yet depletion of a- Si:H(p$^+$) layer is not so severe in this cell such that the impact of the TCO/Si:H interface on V_{OC} is not dominant. This explains why for both cells, V_{OC} is similar as is clearly evident in Figure 11.

On the other hand, V_{OC} is found to be degraded in cell TMB 10/100 with even less doping due to more severe depletion, as depicted in Figure 10. Consequently, the severe degradation of the measured FF to a value around 67% for the low doping sample TMB 10/50 can be attributed to a real resistance enhancement under illumination. This can be further validated by the perfect fitting of the I-V characteristics under illumination that is obtained when the cell series resistance is enhanced from its value of 1.8 Ω cm^2 in the dark to an average value of 3.8 Ω cm^2 throughout the whole voltage range under illumination. On the other hand, the fitting of cell TMB 50/50 can be perfectly obtained keeping the series resistance unchanged under illumination, which agrees very well with the interpretation of negligible resistance enhancement in cells with heavily doped a-Si:H(p$^+$) and with the absence of a Schottky effect, in accordance to the explanation presented in Section 2.

4. Summary and Conclusions

A detailed understanding behind the operation of SHJ devices and what affects their performance is explained based on an analytical model. Such a model is crucial in identifying the exact mechanisms of degradation in SHJ devices and can aid their technological improvement. The SHJ device comprises of two main interfaces, namely, the TCO/a-Si:H interface and the a-Si:H/c-Si interface. By isolating the impact of each interface on the I-V characteristics for SHJ devices under dark and light conditions, it was possible to analyze the root cause of cell performance degradation whether it was mainly from the properties of the TCO/a-Si:H interface or from the a-Si:H/c-Si interface due to thermionic emission. The appearance of an S-shape in the I-V characteristics of SHJ solar cells was also explained based on a rectification action that can be present at the TCO/a-Si:H interface as a result of an inadequate TCO work function. On the other hand, degradation associated with the thermionic emission barrier was shown to be limited to the FF and is caused by a real enhancement in the cell series resistance especially when the free hole concentration in the a-Si:H(p$^+$) layer is not high enough to considerably spill over into the ultrathin intrinsic a-Si:H(i) buffer layer. Under illumination, the latter may be totally depleted which causes a significant increase in the cell series resistance thereby degrading the FF without affecting the value of V_{OC}. This behavior was clearly demonstrated and explained in this work through device

simulations and was experimentally confirmed by studying the I-V characteristics of fabricated SHJ devices in the dark and under illumination. Devices with relatively low doping exhibited an S-shape in the I-V characteristics indicating a Schottky rectification effect and possibly a-Si:H depletion impacting directly the cells' FF and V_{OC}, hence degrading device efficiency.

Data Availability

The data are available on request by contacting the corresponding author, Yaser Abdulraheem (Yaser.abdulraheem@ku.edu.kw).

Conflicts of Interest

The authors declare no conflict of interest.

Authors' Contributions

Authors have made significant contribution to this study and have approved this submission.

Acknowledgments

The work was funded partially by the Kuwait Foundation for the Advancement of Sciences under project code: CN18-15EE-01. This work was partially conducted by the Kuwait University Research Administration General Facilities (project GE01/08).

References

[1] K. Yoshikawa, H. Kawasaki, W. Yoshida et al., "Silicon heterojunction solar cell with interdigitated back contacts for a photoconversion efficiency over 26%," *Nature Energy*, vol. 2, no. 5, pp. 1552–1558, 2017.

[2] M. Ghannam, J. Nijs, R. Mertens, and R. DeKeersmaecker, "A silicon bipolar transistor with a hydrogenated amorphous emitter," in *1984 International Electron Devices Meeting*, pp. 746–748, San Francisco, CA, USA, 1984.

[3] M. Tanaka, M. Taguchi, T. Matsuyama et al., "Development of new a-Si/c-Si heterojunction solar cells: ACJ-HIT (artificially constructed junction-heterojunction with intrinsic thin-layer)," *Japanese Journal of Applied Physics*, vol. 31, pp. 3518–3522, 1992.

[4] M. Taguchi, K. Kawamoto, S. Tsuge et al., "HIT^{TM} cells—high-efficiency crystalline Si cells with novel structure," *Progress in Photovoltaics: Research and Applications*, vol. 8, no. 5, pp. 503–513, 2000.

[5] M. Taguchi, A. Terakawa, E. Maruyama, and M. Tanaka, "Obtaining a $_{\text{higherVoc}}$ in HIT cells," *Progress in Photovoltaics: Research and Applications*, vol. 13, no. 6, pp. 481–488, 2005.

[6] J. Furlan, P. Popović, F. Smole, and M. Topič, "Analytical model of a-Si/c-Si HIT solar cell," *MRS Online Proceedings Library Archive*, vol. 420, p. 261, 2011.

[7] M. Ghannam, G. Shehadah, Y. Abdulraheem, and J. Poortmans, "On the possible role of the interfacial inversion layer in the improvement of the performance of hydrogenated amorphous silicon/crystalline silicon heterojunction solar cells [HIT]," *Solar Energy Materials and Solar Cells*, vol. 132, no. C, pp. 320–328, 2015.

[8] J. P. Kleider, A. S. Gudovskikh, and P. Roca i Cabarrocas, "Determination of the conduction band offset between hydrogenated amorphous silicon and crystalline silicon from surface inversion layer conductance measurements," *Applied Physics Letters*, vol. 92, no. 16, p. 162101, 2008.

[9] R. Varache, J. P. Kleider, W. Favre, and L. Korte, "Band bending and determination of band offsets in amorphous/crystalline silicon heterostructures from planar conductance measurements," *Journal of Applied Physics*, vol. 112, no. 12, p. 123717, 2012.

[10] K. Ghosh, C. Tracy, and S. Bowden, "Experimental and theoretical verification of the presence of inversion region in a-Si/c-Si heterojunction solar cells with an intrinsic layer," in *2012 38th IEEE Photovoltaic Specialists Conference*, pp. 001046–001048, Austin, TX, USA, 2012.

[11] M. Ghannam, Y. Abdulraheem, and G. Shehada, "Interpretation of the degradation of silicon HIT solar cells due to inadequate front contact TCO work function," *Solar Energy Materials and Solar Cells*, vol. 145, no. 3, pp. 423–431, 2016.

[12] T. F. Schulze, L. Korte, E. Conrad, M. Schmidt, and B. Rech, "Electrical transport mechanisms in a-Si:H/c-Si heterojunction solar cells," *Journal of Applied Physics*, vol. 107, no. 2, p. 023711, 2010.

[13] M. Ghannam and Y. Abdulraheem, "Electro-physical interpretation of the degradation of the fill factor of silicon heterojunction solar cells due to incomplete hole collection at the a-Si:H/c-Si thermionic emission barrier," *Applied Sciences*, vol. 8, no. 10, p. 1846, 2018.

[14] M. W. M. V. Cleef, F. A. Rubinelli, and R. E. I. Schropp, "Effects of band offsets ona-Sic:H/c-Si heterojunction solar cell performance," *MRS Online Proceedings Library Archive*, vol. 507, p. 125, 1998.

[15] A. Kanevce and W. K. Metzger, "The role of amorphous silicon and tunneling in heterojunction with intrinsic thin layer (HIT) solar cells," *Journal of Applied Physics*, vol. 105, no. 9, p. 094507, 2009.

[16] M. Stutzmann, D. K. Biegelsen, and R. A. Street, "Detailed investigation of doping in hydrogenated amorphous silicon and germanium," *Physical Review B*, vol. 35, no. 11, pp. 5666–5701, 1987.

[17] S. De Wolf, C. Ballif, and M. Kondo, "Kinetics ofa-Si:H bulk defect anda-Si:H/c-Si interface-state reduction," *Physical Review B*, vol. 85, no. 11, p. 113302, 2012.

[18] R. Varache, C. Leendertz, M. E. Gueunier-Farret, J. Haschke, D. Muñoz, and L. Korte, "Investigation of selective junctions using a newly developed tunnel current model for solar cell applications," *Solar Energy Materials and Solar Cells*, vol. 141, no. C, pp. 14–23, 2015.

[19] E. Centurioni and D. Iencinella, "Role of front contact work function on amorphous silicon/crystalline silicon heterojunction solar cell performance," *IEEE Electron Device Letters*, vol. 24, no. 3, pp. 177–179, 2001.

[20] A. Froitzheim, K. Brendel, L. Elstner, W. Fuhs, K. Kliefoth, and M. Schmidt, "Interface recombination in heterojunctions of amorphous and crystalline silicon," *Journal of Non-Crystalline Solids*, vol. 299, pp. 663–667, 2002.

[21] M. Ghannam and Y. Abdulraheem, "Fundamental constraints imposed by energy barriers on the fill factor and on the efficiency of silicon heterojunction solar cells," *Solar Energy Materials and Solar Cells*, vol. 171, pp. 228–238, 2017.

[22] M. Bivour, S. Schröer, and M. Hermle, "Numerical Analysis of Electrical TCO / a-Si:H(p) Contact Properties for Silicon Heterojunction Solar Cells," *Energy Procedia*, vol. 38, pp. 658–669, 2013.

[23] S. Kirner, M. Hartig, L. Mazzarella et al., "The influence of ITO dopant density on J-V characteristics of silicon heterojunction solar cells: experiments and simulations," *Energy Procedia*, vol. 77, pp. 725–732, 2015.

[24] Y. Hayashi, D. Li, A. Ogura, and Y. Ohshita, "Role of i-aSi:H layers in aSi:H/cSi heterojunction solar cells," *IEEE Journal of Photovoltaics*, vol. 3, no. 4, pp. 1149–1155, 2013.

[25] T. Bearda, A. Umer, S. Jambaldinni et al., "Fabrication of silicon heterojunction cells on 50μm epitaxial substrates," in *33rd European Photovoltaic Solar Energy Conference and Exhibition - EUPVSEC*, pp. 765–767, Amsterdam, The Netherland, 2017.